Quasicontinuum properties of $M1$ spectra in the particle-rotor model

Yong-shou Chen*
Department of Physics, University of Tennessee, Knoxville, Tennessee 37916

G. A. Leander†
UNISOR, Oak Ridge Associated Universities, Oak Ridge, Tennessee 37830
and Florida State University, Tallahassee, Florida 32306

(Received 21 July 1982)

The low-energy $M1$ component that can be observed in quasicontinuum γ-ray spectra from heavy-ion reactions is studied within the core-quasiparticle model. Inclusive one-quasiparticle calculations for sequences of isotopes and isotones indicate how the $M1$ "bumps" vary depending on the structure of the nucleus. Application of the results to higher spins and even-even nuclei is possible on the basis of a spectator quasiparticle hypothesis, which is seen to be adequate qualitatively but not quantitatively.

[NUCLEAR STRUCTURE Calculated $M1$ quasicontinuum γ-ray spectra, deduced dependences on particle and quasiparticle number. Core-quasiparticle coupling models.]

I. INTRODUCTION

For nuclear-structure reasons, the γ rays following compound nucleus formation that are lowest in energy should be largely stretched $M1$ (e.g., Ref. 1). It is of considerable interest to identify and characterize this component of the quasicontinuum γ-ray spectrum in different nuclei and different regions of spin and excitation energy. Recently a number of experiments have been carried out, based on either (i) angular distributions,[2–11] (ii) linear polarization,[12–14] or (iii) the high probability for K-electron conversion by $M1$ radiation at approximately 300 keV in rare-earth nuclei, 300–500 keV in the lead region.[15–18] Evidence for a variety of structure-dependent sources of low-energy $M1$ radiation has been obtained:

(i) *Low-energy "statistical" M1's.* These can only occur very close to the yrast line—otherwise higher-energy statistical transitions dominate—and can therefore largely be identified by discrete-line spectroscopy. Also, they only occur when the yrast line is of a statistical nature—at low spins in odd and odd-odd nuclei and at higher spins in selected nuclei where the rotation takes place around a symmetry axis.[19,20]

(ii) *High-K rotational bands.* The enhancement of $M1$'s and suppression of particularly crossover collective $E2$'s implied by the rotational model[21] when the K of the band is nonzero has been recognized for some time as an important mechanism in HI, $xn\gamma$ cascades (e.g., Refs. 22–24). The $M1$'s are most favored over $E2$'s near the bandheads, for high K, and for small deformation and proton number.

(iii) *Deformation-rotation aligned bands.* It has recently been emphasized by Newton and Sie[3] that the simultaneous requirements of nonzero K and proximity to the yrast line are most likely to be met if one (or more) deformation-aligned quasiparticles provide the K while one (or more) rotation-aligned quasiparticles contribute aligned angular momentum.

(iv) *Relaxation of triaxial modes.* It is a familiar feature of nuclear spectra that gamma bands sometimes deexcite by $M1$ transitions. Also, it has been speculated that there might be closely spaced "wobbling" bands at high spins[25] connected by $M1$ transitions.[26,27]

(v) *High-j levels.* There are large single-particle $M1$ matrix elements within a high-j shell. Hamamoto[28] has recently pointed out that low-energy $M1$'s occur not only in bands based on high-K suborbitals, whose rotational signature splitting is small, but also in decoupled bands based on low-K suborbitals, whose rotational signature splitting is large. Then the unfavored levels of spin $j+2n-1$ may deexcite into the favored levels of spin $j+2n$. Examples of this are known from discrete-line studies (e.g., Ref. 29).

The purpose of this work is to study nuclear structure effects in low-energy $M1$ spectra using

one specific model, the particle-rotor model. The scope of this model is limited by the fact that only a small part of the valence space is described microscopically. Nevertheless, the particle-rotor model has a fairly wide domain of applicability, and in the present work it is used to complement microscopic studies using the random phase approximation[30] and the cranking model.[31,1]

Section II specifies the procedures and parameters employed in the subsequent calculations. Section III A draws on the fact that a reasonably complete and accurate spectrum can be generated for most odd-A nuclei by coupling a quasiparticle in the Nilsson single-particle space to a triaxial rotor core.[32] $M1$ spectra are calculated for chains of isotopes and isotones. In Sec. III B a "spectator quasiparticle" hypothesis, whose validity would be very convenient for any theoretical approach, is studied by comparing results obtained with one and two quasiparticles, respectively. To the extent that the spectator quasiparticle approximation is valid, the results of Sec. III A for odd-A nuclei also apply to doubly odd and doubly even nuclei.

II. THE MODEL

A. Probability spectra

A standardized way is needed to translate a theoretical level spectrum into a quasicontinuum gamma-ray spectrum. In order to characterize the average, or quasicontinuum, properties of a nuclear model we prefer to use a schematic but straightforwardly defined probability spectrum of gamma transitions, as was done previously in cranking calculations,[33,1] rather than to simulate a cascade process with Monte Carlo or master equation techniques. A probability spectrum is obtained by defining *ad hoc* a population distribution P_i over a set of levels labeled by i, and then taking an appropriately weighted sum over all possible gamma transitions. The singles spectrum is obtained as

$$I(E_\gamma)=\sum_i P_i \sum_{E_f<E_i} \sum_{O,\lambda} \alpha(O\lambda;i\rightarrow f)\delta(E_\gamma=E_i-E_f) ,$$

where α is the relative branching from initial state i into final states f. This discrete probability spectrum can be represented as a quasicontinuum simply by binning into finite intervals of E_γ. The total probability spectrum can be decomposed into partial sums, and for example, the $M1$ probability spectrum is obtained by restricting the electromagnetic multipolarity $O\lambda$ to $M1$. The stretched $M1$ probability spectrum is defined as the partial sum where in addition f is restricted to states with one unit of angular momentum more or less than the state i.

Strictly speaking, such a decomposition into electromagnetic multipoles is a mathematical abstraction, and to calculate for example, the angular distribution, it is necessary to take mixing into account explicitly for each transition. As an approximation, however, we assume that each multipole component $O\lambda\mu$ of the probability spectrum has the properties of pure $O\lambda\mu$ radiation. Since stretched $M1$ radiation is most likely to emerge along the axis of nuclear rotation, while the amplitude of stretched $E2$ radiation is largest perpendicular to this axis, we also present spectra below which are obtained as the *difference* between the stretched $M1$ and stretched $E2$ probability spectra. These theoretical results may be compared directly with experimental spectra obtained as the difference between the intensity at 90° and 0°, respectively, relative to the beam axis in HI, $xn\gamma$ experiments.[3,4] The detailed rules for obtaining probability spectra in the present work are as follows:

(i) Population is assigned to levels up to spin $I=\frac{25}{2}$ in the one-quasiparticle case, up to $I=26$ in the two-quasiparticle case, and up to 2 MeV above a smooth yrast envelope or up to the 5th level of given spin, whichever comes first. Levels higher above yrast generally deexcite by higher-energy transitions, and do not contribute much to the low-energy part of the probability spectrum even if they are populated.

(ii) All model states within these limits are equally populated. In the realistic case the population per level is expected to decrease exponentially above yrast, but also the level density is expected to increase very rapidly so that the population per energy interval above yrast may initially increase.[34] The rate of increase in the level density of a finite-matrix model spectrum is not realistic, but drops off rapidly, so the simplistic prescription of equal population (infinite temperature) up to a cutoff at any rate prevents undue weight being attached to the transitions closest to yrast.

(iii) Stretched quadrupole transitions between yrast states are taken out of the probability spectrum. This is done in correspondence with experiments (cf. Refs. 3–5 and 16) where discrete lines are subtracted out of the data.

B. The particle-rotor model

A realistic description of nuclear spectra over a wide range of nuclei and angular momenta is pro-

vided by the well-known particle-rotor model.[35,21] The collective aspects of the nucleus are embodied in a rotor core, while the single-particle aspects arise from a small but appropriately chosen valence space. Several versions of the model are applied in the following for various purposes.

The most complete and widely applicable one, for odd-mass nuclei at low and intermediate spins, is the triaxial rotor plus Nilsson formalism.[32] The triaxial degree of freedom makes it possible to simulate the quadrupole field of transitional as well as deformed cores. The Bardeen-Cooper-Schrieffer (BCS) field is calculated from the Nilsson scheme. The Nilsson levels within a couple of MeV of the Fermi level provide a 1-qp valence space that is realistic and essentially complete for the purposes of the present work.

A simpler variant that is also employed below uses an axially symmetric, rotor core, coupled with a deformed BCS quasiparticle in a valence space spanned by the suborbitals of the $i_{13/2}$ shell. Then the parameters, in addition to the rotor moment of inertia, are the BCS gap parameter Δ, the Fermi level λ, and the splitting of the $i_{13/2}$ suborbitals. The first complete description of the 1-BCS-qp plus rotor formalism may be found in Ref. 36.

The unabridged generalization of the j shell plus rotor formalism to include many-BCS-quasiparticle basis states is presented in Ref. 37. With this approach we have previously been able to obtain a very accurate description of known bands around the first backbend in both even- and odd-mass rotational nuclei.[37,38,33,39]

C. Details of the calculations

This subsection gives the additional information about the parameters which is necessary to make the calculations reproducible. The g factors of the $M1$ operator are taken as $g_R = Z/A$, $g_l = 0$ for a neutron and 1 for a proton, and $g_s = 0.6$ times the g factor of a free nucleon.

The triaxial rotor plus quasiparticle model is based on the Nilsson model as described in Ref. 32. For the ytterbium isotopes we use the "$A=165$" Nilsson parameters,[40] $\kappa_n = 0.0637$ and $\mu_n = 0.42$, and for the $A \sim 130$ region we use parameters extracted from Ref. 41. For the odd-proton $N=72$ isotones we take $\kappa_p = 0.065$, $\mu = 0.57$, the same as for ^{127}Cs in Ref. 42, and for the odd-neutron cerium isotopes we take $\kappa_n = 0.066$, $\mu_n = 0.44$.

The deformation parameters ϵ and ϵ_4 are mostly taken at the potential-energy minima calculated by Ragnarsson *et al.*[43] For $\epsilon \lesssim 0.2$, however, the effect of vibrations must be included. Therefore, effective ϵ values are deduced by interpolation between values deduced from the measured $B(E2;0^+ \rightarrow 2^+)$ in near-spherical $^{122}_{50}\mathrm{Sn}_{72}$, $^{140}_{58}\mathrm{Ce}_{82}$, and $^{158}_{70}\mathrm{Yb}_{88}$, and the theoretical ϵ values in well-deformed $^{132}_{58}\mathrm{Ce}_{74}$ and $^{162}_{70}\mathrm{Yb}_{92}$, respectively.

All Nilsson orbitals within about 2 MeV of the Fermi level are coupled to the core. For the $N=72$ isotones there are six positive parity orbitals, numbers 12–17, and four negative parity orbitals, 14–17. For the cerium isotopes the seven positive parity orbitals 16–22 and seven negative parity orbitals 14–20 are included, leaving out a few in the lightest and heaviest isotopes. Over the ytterbium isotopes, three to five positive parity orbitals out of numbers 23–28 and six or seven negative parity orbitals out of 19–30 are included. A phenomenological "Coriolis attenuation" of the single-particle matrix elements across the Fermi level is achieved by raising the BCS $uu + vv$ factors to power 5.

The rotational moment of inertia and the γ deformation are extracted from the 2_1^+ and 2_2^+ energies of the core, which are defined by interpolation between measured 2^+ energies in the doubly even neighbors.[44] The extrapolated value 0.240 MeV is used for the 2_1^+ energy of ^{132}Nd. In those ytterbium isotopes where the γ bandhead energy is not known, values from isotones are employed. The 2_2^+ energy for $^{128}_{50}\mathrm{Ba}_{72}$ is taken *ad hoc* as 0.8 MeV, and for $^{132}_{60}\mathrm{Nd}_{72}$, $^{126-130}_{58}\mathrm{Ce}$ as 0.9 MeV.

The $M1$ properties of the positive parity levels in ^{161,163,165,167}Yb have been described in a previous paper[29] using an axial rotor plus $i_{13/2}$ quasiparticle approach, where the parameters were adjusted to accurately reproduce the known level energies. The positive-parity contributions to the probability spectra of these Yb isotopes are taken from these earlier calculations, rather than the triaxial model, thereby losing the contribution of the γ bands but gaining accuracy in accounting for the most important levels. In Fig. 1, however, it is the triaxial rotor plus quasiparticle results for ^{161}Yb which are shown for positive as well as negative parity.

In all the $i_{13/2}$ shell plus axial rotor calculations the single-particle matrix elements are evaluated assuming pure $i_{13/2}$ wave functions, but the single-particle energies are taken from the Nilsson model. The probability spectrum is computed with population assigned up to 3.1 MeV above the smoothed yrast line.

The calculations to compare one- and two-quasiparticle contributions from the $i_{13/2}$ shell are

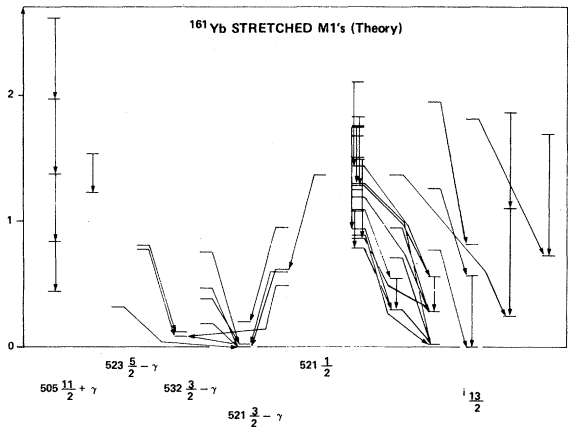

FIG. 1. Partial level scheme from the triaxial rotor plus Nilsson quasiparticle calculation for ^{161}Yb, indicating the levels whose predominant individual decay mode is stretched $M1$.

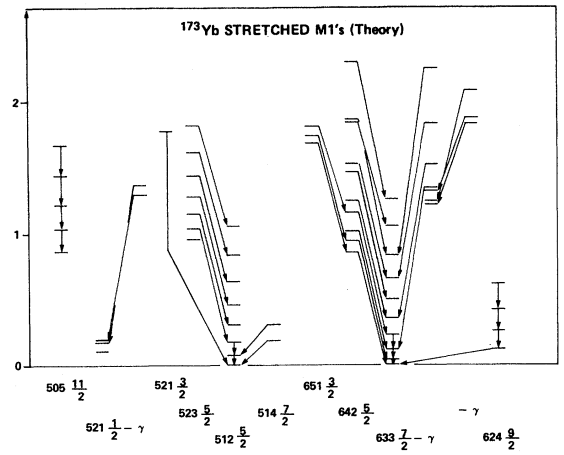

FIG. 2. Same as Fig. 1 but for ^{173}Yb.

carried out with the Fermi level, λ, 0.42 MeV below the $\Omega=\frac{1}{2}$ orbital, then on the $\frac{3}{2}$, $\frac{5}{2}$, $\frac{7}{2}$, and $\frac{9}{2}$ orbitals, respectively. The other parameters are taken as for the corresponding Yb isotopes, except for the moment of inertia. VMI parameters $\theta^{-1}=20$ keV and $C=0.00559$ MeV for two quasiparticles, $C=0.00535$ MeV for one quasiparticle, are employed.

III. RESULTS

A. One-quasiparticle bands

Probability spectra have been calculated for sequences of odd-A nuclei, including the levels up to spin $I=\frac{25}{2}$, in order to see features that distinguish between individual members of a sequence. It is assumed that the triaxial rotor plus Nilsson model is sufficiently accurate for this purpose, although finer details like the exact spacings between bands are known to deviate from experiment by up to a few hundred keV.

Some of the spectroscopic detail underlying the probability spectra is illustrated in Figs. 1 and 2. Partial calculated level schemes are shown for ^{161}Yb and ^{173}Yb, including only those levels whose most probable individual deexcitation mode is a stretched $M1$ transition, as indicated by arrows in Figs. 1 and 2. Many other levels, and other transitions from the levels shown, also contribute to the probability spectrum, though not so strongly. The Nilsson band classification $[Nn_z\Lambda\Omega]$ is indicated below the bands, and $+$ or $-\gamma$ denotes a γ band with $K=\Omega+$ or -2. The decoupled $i_{13/2}$ band structure of ^{161}Yb is displayed in the spirit of the $(\bar{K},\bar{\Omega})$ band classification suggested by Meyer-ter-Vehn.[45]

Several general features can be observed in Figs. 1 and 2. The dominant stretched $M1$ transitions occur at low total excitation energy in these one-quasiparticle systems, all below 2.5 MeV. The reason is that stretched $E2$ transitions dominate at higher spins, where the yrast line is steeper. In-band transitions are primarily responsible for the lowest-energy part of the $M1$ spectrum, and specific interband transitions are mainly responsible at somewhat higher transition energy. The deexcitation of γ bands is also seen to contribute significantly. The obvious systematic differences between Figs. 1 and 2 demonstrate how the $M1$ quasicontinuum spectrum can vary depending on the structure of the nucleus. The larger moment of inertia in ^{173}Yb, and the many high-K levels, is conducive to low-energy $M1$'s. In both nuclei the $i_{13/2}$, or $N=6$, orbitals are of major importance. In ^{173}Yb the transitions are either low energy in band or mostly high-energy interband between the widely separated $i_{13/2}$ suborbitals, whereas no particular transition energies are favored in the decoupled $i_{13/2}$ spectrum of ^{161}Yb. In a decoupled spectrum the core angular momentum R and the rotationally aligned particle angular momentum i are approximate quantum numbers, and $|\Delta i|\leq 1$ favors low-energy transitions. In practice, when energy factors on transition rates are taken into account, this leads to an even spread of the deexcitation from an initial state above the yrast line to a large number of final states giving a broad spectrum of transition energies, since the energy-favored transitions are structure hindered and vice versa.

The one-quasiparticle probability spectra for $^{159-177}$Yb are shown as histograms in Fig. 3. For each odd A, the stretched $M1$ spectrum up to 1 MeV is shown to the left and the stretched $M1$ *minus* the stretched $E2$ spectrum is shown to the right. The latter corresponds roughly to a $90°-0°$ experimental spectrum, and is plotted in Fig. 3 only up to the high-energy edge of the collective "bump" in the quadrupole part of the spectrum. This energy is determined by the cutoff at $I=\frac{25}{2}$ in the present calculation. The vertical scale in all the histograms of Fig. 3 (and Figs. 4 and 5) is determined by the common definition of a probability spectrum given above. There is no relative renormalization between the different diagrams, which can thus be compared on an absolute footing.

Figure 3 displays a broad smooth $M1$ bump for ^{161}Yb, characteristic of the decoupled case, and furthermore a two-bump structure which occurs in ^{173}Yb and the other heavy Yb isotopes. The upper bump is seen to move towards higher energies with increasing neutron number. The $M1$ spectra of $^{159-169}$Yb display local bumps, which may or may not be accurately described by the model, and more significantly a change of skewness within the range $E_\gamma \leq 0.7$ MeV. Higher energies are favored in ^{159}Yb, and lower energies in ^{169}Yb.

The $M1$ minus $E2$ spectrum is generally positive for low energies and negative at the energies of the in-band collective quadrupole transitions. The point where a smoothed curve would go through zero comes lower in energy with increasing neutron number. This is partly due to the change in skewness of the $M1$ bump that was mentioned above, partly to the effect which the increasing moment of inertia has on the energy of the $E2$ bump, and partly to the deformation increase which makes the collective $E2$ transitions more competitive at lower energies.

Figures 4 and 5 are similar to Fig. 3, but for the odd-N isotopes $^{127-137}$Ce and the odd-Z, $N=72$ isotones ^{131}Pr, ^{129}La, ^{127}Cs, ^{125}I, and ^{123}Sb, respectively. All the figures are arranged so that the most deformed nuclei come at the top. The trends with deformation, or equivalently with distance from the closed shells, are similar in Figs. 4 and 5 to those discussed above for Fig. 3. However, the $M1$ bump at 0.7–0.8 MeV in ^{127}Ce is largely due to the γ mode. The nuclei $^{139}_{58}Ce_{81}$ and $^{123}_{51}Sb_{72}$ next to the $N=82$ and $Z=50$ single-shell closures, respectively, do not have any low-lying excitations at all. Consequently, there are no low-energy transitions in the one-quasiparticle spectrum.

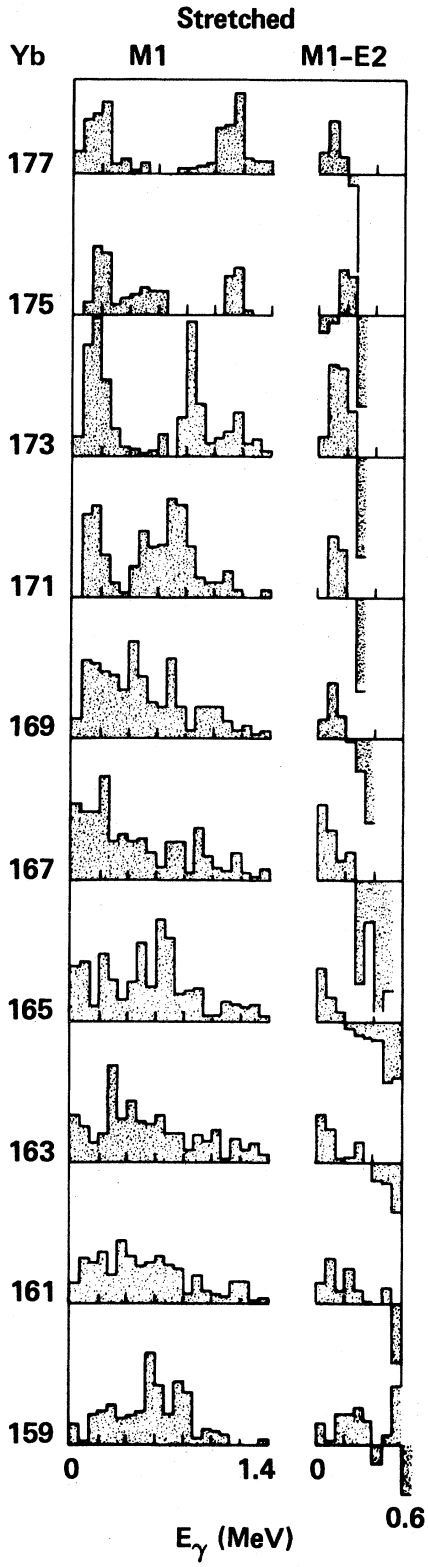

FIG. 3. Stretched $M1$ probability spectra calculated for the odd-N Yb isotopes. The histograms to the right show the same spectra after the calculated stretched $E2$ probability spectrum has been added with a negative sign.

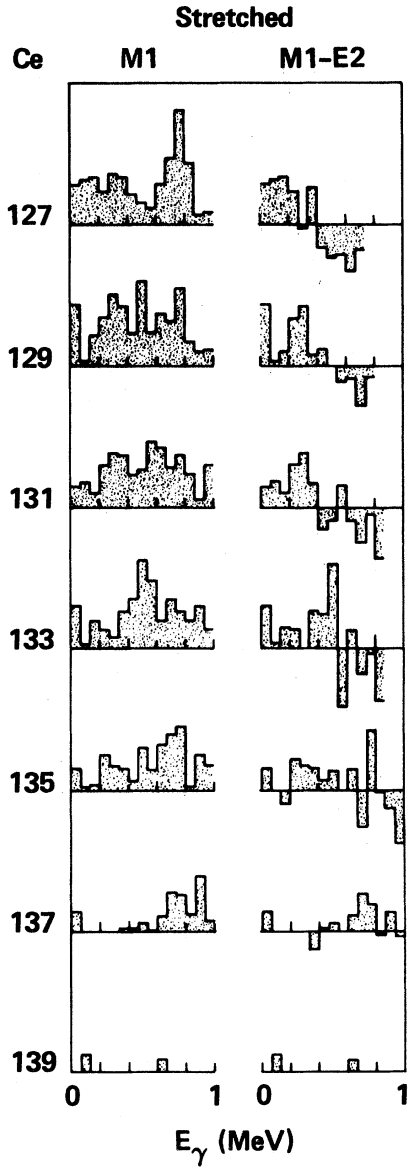

FIG. 4. Same as Fig. 3 but for the odd-N Ce isotopes.

The probability spectra for unstretched $M1$ and $E2$ transitions have also been calculated for all the nuclei in Figs. 3—5. It turns out that the total intensity in all cases is much smaller than for the stretched transitions.

B. Two-quasiparticle bands and the spectator approximation

The excitations of a one-quasiparticle system as studied above correspond approximately to elementary modes, which can be combined in different ways to generate the states of a many-quasiparticle

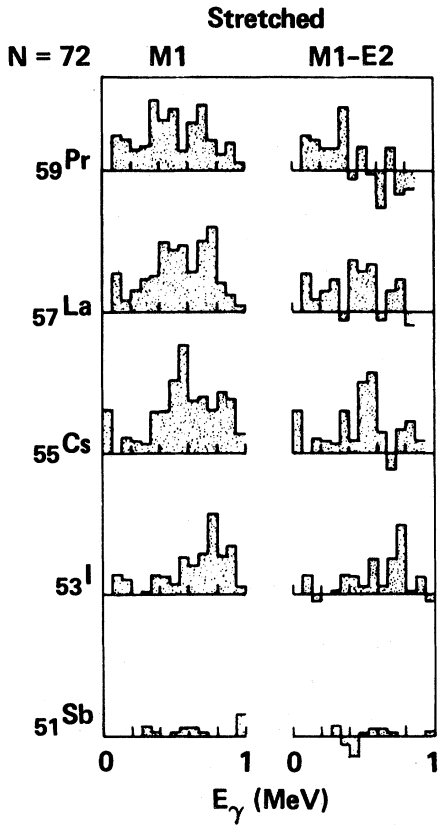

FIG. 5. Same as Fig. 3 but for the odd-Z, $N=72$ isotones.

system. Then, for any given transition, one or zero quasiparticles are active while the rest are spectators. This suggests, for example, that the probability spectrum of a doubly even nucleus is approximately equal to a sum or average of the probability spectra in its odd-A neighbors. A preliminary test of this hypothesis against experiment is shown in Fig. 6. The solid-line bars show the 90°—0° spectrum measured by Newton and Sie[3] in a ^{16}O,4n reaction leading to ^{134}Ce, with discrete lines subtracted out. The dashed-line bars show the stretched $M1$ minus stretched $E2$ probability spectrum obtained from triaxial rotor plus quasiparticle calculations for ^{133}La, ^{133,135}Ce, and ^{135}Pr. The vertical scale is arbitrary. The agreement between theory and experiment is remarkable, with bumps at $E_\gamma \sim 220$ keV and 470 keV and smaller-amplitude oscillations around zero for $E_\gamma = 500-800$ keV. It would be interesting to have experimental data of similar quality in more cases.

In Fig. 7, theory is compared with theory in a sequence of two-quasiparticle and corresponding one-quasiparticle cases. The valence space is restricted to the $i_{3/2}$ shell, where the Fermi level

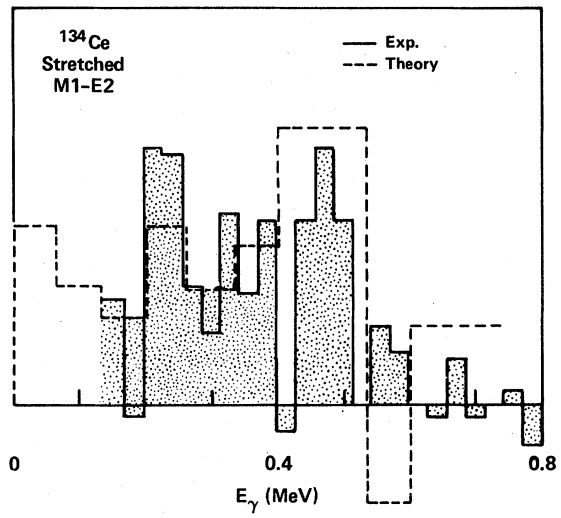

FIG. 6. The 90°−0° spectrum, with discrete lines subtracted out, obtained by Sie *et al.* (Ref. 4) in the reaction ^{122}Sn(^{16}O,4*n*) at 83 MeV (solid line) is compared with a theoretical spectrum, as in Figs. 3−5, summed over the odd-*A* neighboring nuclei (dashed line).

varies from the $\Omega=\frac{9}{2}$ suborbital in the upper case to below the $\Omega=\frac{1}{2}$ orbital in the lowest case in Fig. 7. Exactly the same set of particle-rotor parameters is used for the two-quasiparticle system as for the one-quasiparticle system it is compared with. It appears from Fig. 7 that the similarity between the probability spectra for one and two quasiparticles that is implied by the spectator approximation is fulfilled qualitatively but not quantitatively.

When the Fermi level is low in the shell, i.e., for $N=89$, 91, and 93, the $M1$ intensity is seen to be smaller for two quasiparticles. This is caused by depletion of the two-quasiparticle, $K\neq 0$ bands, where low-energy $M1$'s can occur, due to feeding into lower-lying $K=0$ bands. The depletion takes place mainly through stretched $M1$ transitions of higher energy. The low-lying $K=0$ bands are the S band, with a primary two-quasiparticle component of $(\Omega,-\Omega)$, where Ω is the $i_{13/2}$ suborbital closest to the Fermi level, and at lower spins the ground-state band. An indirect experimental test of the $M1$ strength from $(i_{13/2})^2$ bands to the zero-quasiparticle ground-state band occurs in ^{166}Yb, where the present model predicted correctly the branching between 12^+ and 10^+ from the $12^{+\prime}$ level.[39]

When the Fermi level is higher in the $i_{13/2}$ shell, i.e., for $N=101$ and 105 in Fig. 7, the $M1$ bump in the two-quasiparticle case becomes stronger and wins over the $E2$ bump up to higher energies. In

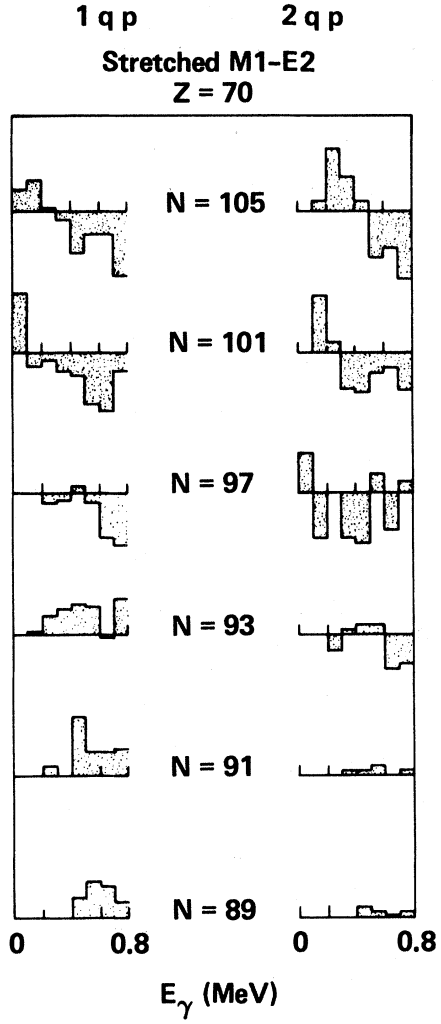

FIG. 7. Stretched $M1$ probability spectrum calculated with the same sets of parameters for one and two quasiparticles, respectively, in an $i_{13/2}$ shell coupled to a rotor. The parameter sets correspond to a sequence of Yb isotopes and differ primarily in that the position of the Fermi level in the $i_{13/2}$ shell changes.

this case the K values in the $K\neq 0$ bands are larger, and the depletion into the low-lying $K=0$ bands is more suppressed by K forbiddenness. Even more importantly, the collective enhancement of $M1$'s is proportional to K^2, and for example, the inequality

$$(\Omega_1+\Omega_2)^2>\Omega_1{}^2+\Omega_2{}^2 \quad (\Omega_1,\Omega_2>0)$$

expresses the fact that the enhancement in a two-quasiparticle band is greater than the sum of the enhancements in the corresponding one-quasiparticle bands. Thus additivity of the probability spectra cannot be expected to hold quantitatively, since the in-band $M1$'s can compete with the

in-band $E2$'s considerably higher up in a two-quasiparticle band. At very low energies, however, the one-quasiparticle $M1$ intensity for $N=101$ and 105 is larger. This is because the lowest spins and spacings which occur in a K band are lower for lower K.

IV. CONCLUSIONS

The gross features of low-energy $M1$ gamma radiation from low and intermediate spin states have been calculated using detailed and rather realistic spectroscopic models. The average features which might be revealed by quasicontinuum measurements are conglomerated from the mass of spectroscopic detail into theoretical "probability spectra." The dominant part of the low-energy transitions, both $M1$ and $E2$, are found to be stretched transitions, i.e., with the maximum spin change allowed by the multipolarity, which emanate from within an MeV or so above the yrast line. The discussion above has illuminated the role of selection rules, e.g., in the nonyrast bands of $(i_{13/2})^1$ and $(i_{13/2})^2$ families of levels. Generally, the gross bump structure of the calculated $M1$ spectrum reflects the specific structure of the nucleus. This is also the case for the $M1$ minus $E2$ spectrum, which of course, also depends on the nuclear-structure dependence of the $E2$ bump.

General consequences of varying deformation are presumably illustrated by the similarities between Figs. 3–5. The total intensity of low-energy $M1$'s is low very near the closed shells, but rises quickly a few nucleon numbers away and then does not change dramatically. The skewness of the lowest-energy bump seems to change characteristically. Far away from closed shells a well localized $M1$ bump may appear at somewhat higher energy, for medium-mass nuclei in the range 0.8–1.2 MeV. The point where the $M1$-$E2$ spectrum changes sign moves gradually toward lower energies.

The results for specific one-quasiparticle nuclei are expected to be qualitatively valid also for spectra taken at somewhat higher spins where many-quasiparticle degrees of freedom come into play, for example, just above the backbend in neighboring doubly even nuclei. Support for this spectator quasiparticle hypothesis comes from a comparison with the unique experimental data available[4] for ^{134}Ce, and from model comparisons between one- and two-quasiparticle systems. Quantitatively, however, the quadratic enhancement of $M1$ collectivity as a function of K is an important nonlinear effect in many-quasiparticle bands. This suggests that also in the cranking model, rather than rely on a generalized version of the spectator quasiparticle approximation as was done in Ref. 1, a high probability for in-band $M1$ transitions could be obtained up to significantly higher spins and energies if the many-quasiparticle high-K bands are constructed explicitly, e.g., with the method of Ref. 46.

Finally we express the hope that experimental studies of such high-K bands in the $M1$ quasicontinuum will prove to be possible, for example, by doing $M1$-$M1$ or $M1$-$E2$ energy-energy correlations.

This work was supported in part by the Office of Energy Research of the U.S. Department of Energy under Contract No. DE-AC05-760R00033 with Oak Ridge Associated Universities, the National Science Foundation under Contract PHY-79-08395, and the Swedish Scientific Research Council.

---

*Permanent address: Institute of Atomic Energy, Academia Sinica, Peking, People's Republic of China.

†Present address: UNISOR, Oak Ridge Associated Universities, Oak Ridge, TN 37830.

[1]Y. S. Chen and I. Hamamoto, Phys. Scr. 24, 763 (1981).

[2]J. O. Newton, S. H. Sie, and G. D. Dracoulis, Phys. Rev. Lett. 40, 625 (1978).

[3]J. O. Newton and S. H. Sie, Nucl. Phys. A334, 499 (1980).

[4]S. H. Sie, R. M. Diamond, J. O. Newton, and J. R. Leigh, Nucl. Phys. A352, 279 (1982).

[5]S. H. Sie, J. O. Newton, and R. M. Diamond, Nucl. Phys. A367, 176 (1982).

[6]M.-A. Deleplanque *et al.*, Phys. Rev. Lett. 41, 1105 (1978).

[7]F. Folkmann *et al.*, Nucl. Phys. A361, 242 (1981).

[8]P. Aguer *et al.*, Phys. Scr. 24, 140 (1981).

[9]T. L. Khoo *et al.*, Phys. Scr. 24, 283 (1981).

[10]C. V. K. Baba *et al.*, Phys. Scr. 24, 290 (1981).

[11]M. Jääskeläinen *et al.*, Phys. Scr. (to be published).

[12]J. P. Vivien *et al.*, Phys. Lett. 85B, 325 (1979).

[13]W. Trautmann *et al.*, J. Phys. 41, Suppl. C10–249 (1980).

[14]H. Hübel *et al.*, Z. Phys. A 297, 237 (1980).

[15]D. Chmielewska, Z. Sujkowski, R. V. F. Janssens, and M. J. A. de Voigt, Nucl. Phys. A366, 142 (1981) and

Refs. 4–13 therein.
[16]L. Westerberg *et al.*, Phys. Rev. Lett. 41, 96 (1978).
[17]S. J. Feenstra *et al.*, Phys. Lett. 80B, 183 (1979).
[18]H. J. Karwowski *et al.*, Phys. Rev. Lett. 47, 1251 (1981).
[19]A. Bohr and B. R. Mottelson, Phys. Scr. 10A, 13 (1974).
[20]G. Andersson *et al.*, Nucl. Phys. A268, 205 (1976).
[21]A. Bohr and B. R. Mottelson, *Nuclear Structure* (Benjamin, New York, 1975), Vol. 2.
[22]S. M. Fergusson, H. Ejiri, and I. Halpern, Nucl. Phys. A188, 1 (1972).
[23]M. Wakai, M. Sano, and A. Faessler, Contributions to the International Conference on Nuclear Behaviour at High Angular Momentum, Strasbourg, 1980 (unpublished), p. 77.
[24]H. Ejiri, Phys. Scr. 24, 130 (1981).
[25]B. R. Mottelson, Proceedings of the Nuclear Structure Symposium, Joutsa, 1970 (unpublished).
[26]R. J. Liotta, Phys. Scr. 21, 135 (1980).
[27]Ph. Hubert *et al.*, J. Phys. 41, Suppl. C10–139 (1980).
[28]I. Hamamoto, Phys. Lett. 102B, 225 (1981).
[29]Y. S. Chen, L. L. Riedinger, and G. A. Leander, Phys. Lett. 113B, 124 (1982).
[30]C. G. Andersson, J. Krumlinde, Z. Szymański, and G. Leander, Nucl. Phys. A361, 147 (1981).
[31]I. Hamamoto and H. Sagawa, Nucl. Phys. A327, 99 (1979).
[32]S. E. Larsson, G. Leander, and I. Ragnarsson, Nucl. Phys. A307, 189 (1978).
[33]G. Leander, Y. S. Chen, and B. S. Nilsson, Phys. Scr. 24, 164 (1981).
[34]Y. S. Chen, M. W. Guidry, and G. A. Leander (unpublished).
[35]A. Bohr and B. R. Mottelson, K. Dan. Vidensk. Mat. Fys.-Medd. 27, No. 16 (1953).
[36]E. Osnes, J. Rekstad, and O. K. Gjøtterud, Nucl. Phys. A253, 45 (1975).
[37]J. Almberger, I. Hamamoto, and G. Leander, Phys. Scr. 22, 331 (1980).
[38]J. Almberger, I. Hamamoto, and G. Leander, Nucl. Phys. A333, 184 (1980).
[39]W. Walus *et al.*, Phys. Scr. 24, 324 (1981).
[40]S. G. Nilsson *et al.*, Nucl. Phys. A131, 1 (1969).
[41]S. E. Larsson, G. Leander, I. Ragnarsson, and N. G. Alenius, Nucl. Phys. A261, 77 (1976).
[42]Ch. Droste *et al.*, Nucl. Phys. A381, 98 (1980).
[43]I. Ragnarsson *et al.*, Nucl. Phys. A233, 329 (1974).
[44]M. Sakai and A. C. Rester, At. Data Nucl. Data Tables 20, 441 (1977).
[45]J. Meyer-ter-Vehn, Nucl. Phys. A249, 111 (1975).
[46]A. Faessler and M. Płoszajczak, Phys. Rev. C 16, 2032 (1977).